Published in final edited form as:
Biochemistry. 2013 July 9; 52(27): . doi:10.1021/bi400563c.

A distal mutation perturbs dynamic amino acid networks in dihydrofolate reductase

David D. Boehr[#1,3], **Jason R. Schnell**[#1,4], **Dan McElheny**[#1,5], **Sung-Hun Bae**[1,6], **Brendan M. Duggan**[1,7], **Stephen J. Benkovic**[2], **H. Jane Dyson**[1], and **Peter E Wright**[*,1]

[1]Department of Integrative Structural and Computational Biology and the Skaggs Institute for Chemical Biology, The Scripps Research Institute, 10550 North Torrey Pines Road, La Jolla, CA 92037, USA

[2]The Pennsylvania State University, Department of Chemistry, 414 Wartik Laboratory, University Park, PA 16802, USA

[#] These authors contributed equally to this work.

Abstract

Correlated networks of amino acids have been proposed to play a fundamental role in allostery and enzyme catalysis. These networks of amino acids can be traced from surface-exposed residues all the way into the active site, and disruption of these networks can decrease enzyme activity. Substitution of the distal Gly121 residue in *E.coli* dihydrofolate reductase results in up to a 200-fold decrease in the hydride transfer rate despite the fact that the residue is located 15 Å from the active-site center. In the present study, NMR relaxation experiments are used to demonstrate that dynamics on the ps-ns and μs-ms timescales are changed significantly in the G121V mutant of dihydrofolate reductase. In particular, ps-ns timescale dynamics are decreased in the FG loop (containing the mutated residue 121) and the neighboring active-site loop (the Met20 loop) in the mutant compared to wild-type enzyme, suggesting that these loops are dynamically coupled. Changes in methyl order parameters reveal a pathway by which dynamic perturbations can be propagated more than 25 Å across the protein from the site of mutation. All of the enzyme complexes, including the model Michaelis complex with folate and $NADP^+$ bound, assume an occluded ground state conformation, and we do not observe sampling of a higher energy closed conformation by ^{15}N R_2 relaxation dispersion. This is highly significant, since it is only in the closed conformation that the cofactor and substrate reactive centers are positioned for reaction. The mutation also impairs μs - ms timescale fluctuations that have been implicated in product release from the wild type enzyme. Our results are consistent with an important role for Gly121 in controlling protein dynamics critical for enzyme function and further validate the dynamic energy landscape hypothesis of enzyme catalysis.

[*]Corresponding author address: Department of Integrative Structural and Computational Biology, The Scripps Research Institute, 10550 North Torrey Pines Road, La Jolla, California, 92037, U.S.A.; phone (858) 784 9721; wright@scripps.edu.
[3]Present Address: Department of Chemistry, Pennsylvania State University, University Park PA 16802, USA.
[4]Present Address: Department of Biochemistry, University of Oxford, South Parks Road, Oxford, OX1 3QU, U.K.
[5]Present Address: Department of Chemistry, University of Illinois at Chicago, 845 West Taylor Street - MC 111 - Chicago IL - 60607
[6]Present Address: Nymirum, 3510 W Liberty Rd Ann Arbor, MI 48103
[7]Present Address: UC San Diego Skaggs School of Pharmacy and Pharmaceutical Sciences, 9500 Gilman Drive, La Jolla, CA 92093

SUPPORTING INFORMATION AVAILABLE Tables showing excluded residues, model-free diffusion parameters, methyl order parameters, kinetic and thermodynamic parameters and dynamic chemical shift differences, and plots of ^{15}N relaxation parameters, diffusion coefficients and relaxation dispersion curves. Supporting materials may be accessed free of charge online at http://pubs.acs.org.

(Introduction)

There is now a significant body of evidence supporting a functional role for protein dynamics in biologically-important processes such as protein-protein interactions, allosteric regulation and enzyme catalysis.[1–8] These studies suggest that protein motions can be directed towards a functional purpose (e.g. capture or release of a ligand). It has been suggested that coupled networks of amino acids exist in proteins such that motions in distant regions can influence events at a functional site.[3,7,9–13] It has also been shown that disruption of these proposed networks leads to severe impairment of protein function[3,8], suggesting new mechanisms of allostery whereby changes in global structure and/or protein dynamics can significantly influence biological activity, even in monomeric or traditionally `non-allosteric' proteins.[14–18] These insights offer additional complexities to protein engineering and new opportunities for drug design.

One of the enzymes in which coupled networks of protein motion have been proposed to play a major role in catalytic function is *Escherichia coli* dihydrofolate reductase (DHFR).[9,12,19–22] DHFR is a small (18 kD) enzyme that catalyzes the reduction of folate (FOL) to dihydrofolate (DHF), and dihydrofolate (its physiological substrate) to tetrahydrofolate (THF) using the cofactor NADPH.[23] The rate-limiting step in the steady state catalytic cycle is release of product THF, which is coupled to rebinding of NADPH to the enzyme.[24] Structural and kinetic studies suggest that control over substrate and cofactor binding is mediated by several flexible loops that surround the active site.[25–28] The loops are referred to as the Met20 (residues 9–24), FG (116–132) and GH (142–150) loops (Figure 1). These loops assume three distinct conformations in the crystalline state, denoted occluded, closed, and open,[25] although only the occluded and closed loop conformations appear to be significantly populated in solution.[29] In substrate complexes, the Met20 loop is occluded, with the central region (residues Met16 and Glu17) flipped into the cofactor binding pocket such that the nicotinamide ring is sterically occluded from binding. However upon binding cofactor, Met16 and Glu17 move out of the nicotinamide binding pocket, residues Met16-Ala19 adopt a type III' β-hairpin, and the side-chains of Asn18 and Met20 pack over the pterin ring to form the closed conformation. Only the closed conformation allows proximal positioning of the cofactor and substrate reactive centers and therefore it is the closed conformation that must be adopted in the Michaelis complex.[25,29] The occluded and closed Met20 loop conformations are stabilized by unique hydrogen bonding networks to the GH and FG loops, respectively.

On the basis of mixed quantum mechanical/classical molecular dynamics simulations (QMMM), it has been proposed that a network of coupled promoting motions, involving both amino acid residues in the active-site and on the exterior of the protein, is important for DHFR catalysis.[9] In particular, Gly121 and Asp122 in the FG loop appear to participate in a network of correlated protein motions that act to compress the reaction coordinate and stabilize the transition-state.[9,19–21] Consistent with this hypothesis, Gly121 and Asp122 mutants exhibit significantly decreased hydride transfer rates.[26,27,30–34] For example, mutation of Gly121 to Val results in a 40-fold decrease in NADPH binding affinity and a 200-fold reduction in the hydride transfer rate, despite the fact that Gly121 is located ~ 15 Å from the active site[34] (Figure 1). In addition, the G121V mutation results in a 7-fold decrease in the rate of product release.[34] Moreover, enzymes with double and triple mutations involving Gly121 and other proposed members of the network (e.g. Met42) showed synergistic decreases in hydride transfer rates, suggesting that the amino acid residues in the network are kinetically and thermodynamically coupled.[21,35] Both molecular dynamics simulations[21,36] and experimental kinetic isotope effects suggest different gating motions or conformational sampling between WT and mutant enzyme.[37–39]

These results are especially interesting in light of the fact that Gly121 appears to be the most flexible residue in the enzyme. Previous NMR relaxation studies of the backbone dynamics of DHFR identified large amplitude motions on the nanosecond time scale for Gly121 and other residues in the FG loop.[40–42] NMR R_2 relaxation dispersion experiments have also shown that Gly121 is conformationally mobile on the μs-ms timescale for most complexes of DHFR.[43,44] These results raise questions about the role of flexibility and protein motion in DHFR catalysis, and specifically, about the role of Gly121 in the catalytic cycle of DHFR.

To further explore the relationship between catalysis and protein dynamics in DHFR, we used NMR relaxation experiments to study protein dynamics from the ps to ms timescales for four complexes of G121V DHFR – E:FOL:$NADP^+$, a model for the Michaelis complex (E:DHF:NADPH); E:FOL, a model for the binary product complex (E:THF); and the two product ternary complexes, E:THF:$NADP^+$ and E:THF:NADPH. The largest motional differences between WT and G121V DHFR on the ps-ns timescale are for residues located in the FG and Met20 loops, providing evidence that motions in the active-site loops are coupled. These changes in dynamics are propagated more than 25 Å across the protein to the adenosine binding domain. Moreover, in all four complexes, the G121V enzyme populates an occluded ground state[29] and does not appear to significantly sample the catalytically-competent closed conformation on the μs-ms timescale (population <1% of the conformation ensemble). These results help to explain the differences in ligand affinities and hydride transfer rates between WT and G121V enzymes, and serve as a further validation of the dynamic energy landscape hypothesis of enzyme catalysis.[8,45,46]

Materials and methods

Sample Preparation

WT and G121V DHFR were overexpressed and purified as described previously.[26,40,45] Samples for resonance assignments consisted of ~1.0 – 1.5 mM solution of G121V DHFR uniformly labeled with $^{15}N/^{13}C$ or $^{2}H/^{15}N/^{13}C$. Samples for R_1, R_2, and heteronuclear NOE experiments consisted of ~1.5 mM protein uniformly labeled with ^{15}N. R_2 relaxation dispersion experiments were performed with 1 mM uniformly $^{2}H,^{15}N$-labeled DHFR.

Samples for measurement of methyl ^{2}H relaxation consisted of 2.5–3.0 mM solution of G121V protein uniformly labeled with ^{15}N and ^{13}C, and with partial random deuteration at all nonexchangeable proton sites. Deuteration to ~45% results in a large fraction of methyls with a single deuterium spin ($^{13}CH_2^2H$) and was achieved by growth of transformed *E. coli* BL21-DE3 cells on 65% D_2O. The extent of deuteration was estimated by MALDI mass spectrometry.

NMR samples for E:FOL and E:FOL:$NADP^+$ were prepared in argon flushed buffer, pH 6.8, containing 50 mM potassium phosphate, 100 mM KCl and 1 mM DTT, and stored in amberized tubes sealed with a septum. FOL and $NADP^+$ were added to 6-fold and 10-fold excess over protein, respectively. THF and NADPH are more susceptible to oxidation; therefore buffer was thoroughly degassed through freeze-pump-thaw cycles using a vacuum apparatus and ascorbic acid was added to act as an oxygen scavenger. The final samples for the E:THF:$NADP^+$ or E:THF:NADPH complexes contained 1 mM DHFR, 10 mM $NADP^+$/ 10 mM NADPH, 6 mM THF, 1 mM DTT, 25 mM KCl and 10% D_2O in 70 mM KP_i pH 7.6. The samples were placed in amberized NMR tubes, subjected to vacuum again, overlaid with argon and flame-sealed.

Resonance Assignments

Backbone amide assignments for the G121V complexes were determined using either standard[47–49] and/or deuterium-decoupled[50] versions of HNCA and HNCACB for ^{13}C, ^{15}N-labeled and ^{2}H, ^{13}C, ^{15}N-labeled mutant proteins, respectively. In some cases (E:FOL and E:FOL:$NADP^+$), additional experiments including HN(CO)CA, HN(CO)CACB and/or CBCA(CO)NH were used to confirm assignments. Methyl resonances for the E:FOL complex were assigned from three-dimensional ^{15}N TOCSY-HSQC[51] and (H)C(CO)NH / H(CCO)NH spectra.[52]

R_1, R_2 and heteronuclear NOE

^{15}N relaxation data on the WT and G121V E:FOL complexes were recorded at 306.4 K at three fields using Bruker Avance 500 MHz, DRX 600 MHz, and DMX 750 MHz spectrometers (Supporting Information Figure S1). The pulse sequences closely followed those of Farrow et al.[53] with sensitivity enhancement and coherence selection via pulsed-field gradients. NMR samples of the two complexes were made fresh within a month of each other using the same folate stock, and relaxation parameters were collected back to back on the same spectrometers to ensure the least amount of sample and spectrometer variability. Choice of delays in the R_1 and R_2 experiments were based on the 2-delay Cramer-Rao approach[54] in which the shortest experimentally accessible delay is recorded along with a second delay at 1.3× the relaxation time, taken as the trimmed mean (T_{mean}) for all residues. Optimal delays were chosen based on preliminary measurements in which the full decay was sampled. The R_1 experiments were recorded with a short delay of 10 ms and a long delay (~1.3 * T_{mean}) of 770 ms (500 MHz), 1000 ms (600 MHz), or 1606 ms (750 MHz). The R_2 measurements were recorded with a short delay of 4 ms and a long delay (~1.3 * T_{mean}) of 120 ms (500, 600 MHz) or 108 ms (750 MHz). Three (two) duplicates at the short delay and five (four) duplicates at the long delay at 500 MHz and 750 MHz (600 MHz) allowed direct estimation of the uncertainty in peak intensity on a residue-by-residue basis. The R_1 and R_2 rates were determined from a two parameter exponential fit to the peak heights using the program CurveFit.[55,56] R_2 data obtained previously on the same WT sample at 600 MHz using a traditional sampling scheme with 10 delays spaced between the shortest attainable delay to roughly 2.5*T_{mean} were compared to R_2 data measured using the Cramer-Rao method. The R_2 values derived from the two sampling schemes were very similar. The R_2 average and standard deviation was 10.66 ± 1.16 s^{-1} and 10.73 ± 1.26 s^{-1}, and the range of R_2 values was 6.10 to 16.60 s^{-1} and 5.82 to 16.66 s^{-1} for traditional and Cramer-Rao sampling schemes, respectively.

The {^{1}H}-^{15}N NOE was recorded five (600 MHz) or six (500 MHz, 750 MHz) times with a saturation period consisting of 120° ^{1}H pulses spaced 18 ms apart for a total of 3.0 s.[57] The saturated and unsaturated spectra were recorded in an interleaved manner to minimize systematic errors. A relaxation delay of 2.6 s was used for all ^{15}N relaxation experiments.

COPED analysis

An accurate description of the internal motions requires that deviations from isotropic molecular tumbling be taken into account.[58] Previous work has identified a small degree of anisotropic molecular rotation in *E. coli* DHFR that, if neglected, can lead to erroneous fitting of exchange terms (R_{ex}).[59] Care must be taken that residues with genuine exchange terms or large amplitude internal motions are not included in the initial description of the molecular diffusion parameters.[60] With this in mind, the COPED approach[59] was used to determine the diffusion tensor and rotational correlation time τ_m through a comparison of the experimental local diffusion coefficients derived from relaxation data and the diffusion coefficients predicted from a hydrodynamic model. In this way, residues with significant contributions to relaxation rates from picosecond/nanosecond or μs-ms motions were

identified and excluded from the initial calculations of the molecular diffusion parameters. Predicted local diffusion coefficients ($D_{i(pred)}$) were calculated using the in-house program MASH (written by Ishwar Radhakrishnan) which incorporates the HYDRO suite of programs.[61] The protein was modeled as a set of beads with radius 3.09–3.11 Å centered on the Cα atoms. The exact bead radius was chosen so as to minimize the error function $\chi^2 = (D_{i(exp)} - D_{i(exp)})/\sigma^2$, where σ is the uncertainty in $D_{i(exp)}$. The experimental local diffusion coefficients were calculated from local correlation times estimated from the R_2/R_1 ratio using the program `tmest'.[62] Residues with a positive or negative deviation from $D_{i(pred)}$ and a $\chi^2 > 6$ at either 500 or 600 MHz were identified as undergoing ps-ns or μs-ms internal motions, respectively, and excluded from determination of the initial diffusion tensor. These residues were later re-introduced for determination of model-free parameters. As shown in Supporting Information Table S1, the lists of excluded residues are similar for WT and G121V DHFR. However, FG loop residues 120–122, which are excluded for WT because of ps-ns motions, no longer exhibit these motions in G121V DHFR. Instead, residues 119 and 122 are excluded because of predicted μs-ms motions. Residues exhibiting {1H}-^{15}N NOE < 0.65 were also excluded from calculation of the molecular diffusion parameters. The initial estimates of τ_m based on ^{15}N R_2/R_1 ratios of the retained residues were 8.72 and 8.64 ns for WT and G121V DHFR, respectively. Final τ_m values optimized using the model-free results (Supporting Information Table S2) differed only slightly. The program quadric_diffusion was used to estimate $D_{\parallel} / D_{\perp}$ and rotate the crystal structure along the principal component of the diffusion tensor.

Anisotropic model-free analysis

The relaxation data sets for the WT and G121V E:FOL complexes were analyzed independently using an axially symmetric diffusion tensor and the program ModelFree 4.15. Backbone amide vector orientations determined from the crystal structure of DHFR in complex with folate (1RX7)[25] were used for both WT and G121V DHFR (see Results). Although an NH bond length of 1.04 Å and an ^{15}N CSA of −160 ppm may be more physically reasonable,[63,64] the combination of 1.02 Å and −172 ppm was used in the present study to facilitate comparison with earlier work. With these parameters, S^2values reflect both librational motions of the peptide plane and quantum mechanical zero-point motions. The CSA for the $^{15}N^{\varepsilon}$ atom in the tryptophan indole ring was set to −126 ppm. For each complex, the relaxation data at multiple fields were fit simultaneously using the extended Lipari-Szabo formalism.[65] The appropriate dynamic model for each residue (Model 1: S^2; Model 2: S^2, τ_e; Model 3: S^2, R_{ex}; Model 4: S^2, τ_e, R_{ex}; Model 5:, S^2_f, S^2_s,τ_e) was selected with an in-house program using the Bayesian information criterion for model selection (Supporting Information Table S3).[66–68]

^{2}H methyl side-chain relaxation

Dynamics of methyl-containing side chains in the G121V E:FOL complex were probed using quadrupolar ^{2}H relaxation. Relaxation datasets were recorded on Bruker DRX spectrometers operating at ^{1}H frequencies of 600 and 800 MHz (92 and 123 MHz for ^{2}H) using published pulse sequences.[69] Due to a large variation in rates, the 2-delay Cramer-Rao method for sampling the decay could not be applied. The $R_1(I_zC_zD_z)$ experiments were recorded with delays of 0.05*, 4, 14, 20, 27, 35*, 44, 64 and 75* ms. The $R_{1\rho}(I_zC_zD_y)$ experiments were recorded with delays of 0.25*, 2, 3.5, 5*, 7, 9, 14*, 17 and 28 ms. The asterisks denote delays at which data were collected in duplicate for estimation of peak uncertainty. The contribution from spin flips in neighboring protons $R_1(I_zC_z)$ was measured using delays of 0.135*, 11, 30, 50, 80*, 110, 140, 170 and 210* ms and subtracted from the observed deuterium relaxation rates to obtain $R_1(^2H)$ and $R_2(^2H)$. All relaxation rates were determined from a two parameter fit to peak heights using the program CurveFit.[70] Data points with intensities less than twice the spectral noise were excluded from the fit.[71]

^{2}H relaxation rates were fit to model-free parameters S^2_{axis} and τ_e, where S^2_{axis} reflects motion about the vector between the methyl carbon and the adjacent bonded carbon. S^2_{axis} is derived from S^2 scaled by $[(3\cos^2\theta - 1)/2]^2$ to remove the contribution from free methyl rotation, where θ is the angle between the C-C_{methyl} bond and the C_{methyl}-^{2}H bond (109.5°). Fitting was accomplished using ModelFree with the appropriate equations for ^{2}H quadrupolar relaxation[72] and with the quadrupolar coupling constant (e^2qQ/h) set to 167 kHz.[73] Rotational correlation times were estimated from the ratio of backbone amide ^{15}N relaxation rates R_1 and R_2[74]$_2$ collected on the same samples. The methyl model-free parameters are summarized in Supporting Information Table S4.

^{15}N R_2 relaxation dispersion

^{15}N R_2 dispersion experiments were performed for G121V E:FOL, E:FOL:NADP$^+$, E:THF:NADP$^+$ and E:THF:NADPH complexes at ^{1}H spectrometer frequencies of 500 and 800 MHz using constant-time relaxation-compensated CPMG (Carr-Purcell-Meiboom-Gill) pulse sequences.[43,75] The total relaxation time was 40 ms for the E:FOL:NADP$^+$, E:THF:NADP$^+$ and E:THF:NADPH complexes, and 80 ms for the E:FOL complex. The R_2 relaxation dispersion data were fit simultaneously at the two frequencies using the in-house computer program GLOVE with the following series of equations describing conformational exchange between two sites, A and B:

$$\boldsymbol{R}_2\left(1/\tau_{CP}\right)=\boldsymbol{R}_2^0+\frac{\mathbf{1}}{2}\left[k_{ex}-\frac{\mathbf{1}}{\tau_{CP}}\cosh^{-1}\left[D_+\cosh\left(\eta_+\right)-D_-\cos\left(\eta_-\right)\right]\right] \quad (1)$$

in which,

$$D_\pm=\frac{1}{2}\left[\pm 1+\frac{\psi+2\Delta\omega^2}{\left(\psi^2+\zeta^2\right)^{1/2}}\right]^{1/2} \quad (2)$$

$$\eta_\pm=\frac{\tau_{CP}}{2}\left[\pm\psi+\left(\psi^2+\zeta^2\right)^{1/2}\right]^{1/2} \quad (3)$$

where $\psi=k_{ex}^2-\Delta\omega^2$, $\zeta=-2\Delta\omega k_{ex}(p_A-p_B)$, τ_{CP} is the time between successive 180° pulses in the CPMG pulse train, R_2^0 is the R_2 relaxation rate in the absence of conformational exchange, p_A and p_B are the populations of the ground- and excited-state conformations respectively ($p_A + p_B = 1$), and $\Delta\omega$ is the chemical shift difference between substates A and B. Rate constants for the ground-to-excited state (k_{AB}) and excited-to-ground state (k_{BA}) transitions can be determined by $p_B.k_{ex}$ and $p_A.k_{ex}$ respectively. Residues generally fit in one of two clusters, one containing residues in the active-site loops and/or the substrate/product/cofactor binding sites, and the other consisting of a small cluster of residues near the C-terminus (residues 129–134, 157–159). Each cluster was fit with global k_{ex} and p_Ap_B values while allowing $\Delta\omega$ values to vary for each residue. The clusters showed significantly different p_B, k_{AB} and k_{BA} values (Table 1) (k_{ex} and p_Ap_B values are shown in Supplementary Table S5). The sign for $\Delta\omega$ was determined by comparing HSQC and HMQC spectra[76]; $\Delta\omega$ values are listed in Supporting Information Table S6.

Temperature dependence of μs-ms timescale dynamics

The enthalpy (ΔH) and entropy ($-T\Delta S$) energy differences between the excited- and ground-state conformations were estimated from the temperature dependence of the conformational exchange equilibrium constant using van't Hoff analysis:

$$\ln K = -\Delta H/RT + \Delta S/R \quad (4)$$

where K is equal to k_{BA}/k_{AB}. Reported errors are based on jackknife simulations.[43,45] The activation barriers were estimated using transition-state theory:

$$k = (k_B T/h)\, e^{\Delta S^{\ddagger}/R} e^{-\Delta H^{\ddagger}/RT} \quad (5)$$

where k is the rate constant from R_2 relaxation dispersion (k_{AB}), k_B is Boltzmann's constant, h is Planck's constant, R is the universal gas constant, T is temperature, $\Delta S^{\ddagger}$ is the entropy of activation and $\Delta H^{\ddagger}$ is the enthalpy of activation.

Results

Chemical shift differences between WT and G121V complexes

Differences in backbone amide chemical shifts between the WT and G121V DHFR complexes are shown in Figure 2. For the E:FOL, E:THF:$NADP^+$ and E:THF:NADPH complexes, the $^1H^N$ and ^{15}N chemical shift differences between WT and G121V complexes are small for most residues (Figure 2A, C, D), indicating that the G121V and WT enzymes adopt the same occluded conformation. Not surprisingly, residues in the FG loop near the site of mutation show large changes in chemical shift, while small chemical shift changes are observed for some residues in the Met20 loop (Ala9, Val10, Arg12, Val13, Ile14, Gly15) indicative of subtle adjustment of the backbone to accommodate the bulky Val121 side chain. In contrast to the WT E:FOL:$NADP^+$complex, which adopts a closed Met20 loop conformation, the E:FOL:$NADP^+$complex of the G121V mutant remains occluded. With the exception of Ala7, which hydrogen bonds differently with folate and THF[29] only small chemical shift differences are observed between the E:FOL:$NADP^+$complex and the occluded E:THF:$NADP^+$ complex of G121V (Figure 2B, red curve). In contrast, there are large differences in chemical shift for residues throughout the Met20 loop (residues 9–24) between the closed WT E:FOL:$NADP^+$ complex and the occluded G121V E:FOL:$NADP^+$ complex (Figure 2B).

Backbone ps-ns timescale motions in the G121V E:FOL complex

The ps-ns timescale dynamics of DHFR depend primarily on the backbone conformation[42], whereas the μs-ms timescale dynamics are highly ligand specific.[45,77] Backbone amide and tryptophan imino ^{15}N R_1, R_2 relaxation rates and {1H}-^{15}N NOEs were acquired under identical conditions for the E:FOL complexes of WT and G121V DHFR, both of which adopt occluded ground state conformations (Supporting Information Figure S1).

After acquisition of the R_1, R_2, and heteronuclear NOE data reported in this paper, Ferrage et al.[78] demonstrated that systematic errors in the magnitude of the NOE can result from use of a 120° flip angle for ^1H irradiation. Based on the simulations of Ferrage et al., the measured rotational correlation time of DHFR (~8.6 ns), and the 18 ms spacing between successive 120° pulses in our experiments, we estimate that any errors introduced would be smaller than the uncertainties in the NOE measurements for residues with $S^2 \geq 0.7$. For residues in flexible loops, with $S^2 < 0.7$, systematic errors could occur in τ_e; however, S^2 values are much more robust and are influenced only slightly by the choice of flip angle.[78] In analyzing our data for residues in flexible loops, differences in dynamics between WT and G121V DHFR were only considered to be significant if a substantial difference was observed in the order parameters ($\Delta S^2 = 0.06 – 0.18$). Further, the relaxation data for the WT and G121V complexes were acquired under identical conditions and residues that differ in

S^2 and τ_e can thus be identified with high confidence, even if the absolute magnitude of τ_e for residues in flexible loops is subject to systematic error.

Anisotropic model-free analysis[65,79,80] was performed using ^1H-^{15}N bond orientations determined from the crystal structure of WT DHFR bound to folate (1RX7) for both WT and G121V relaxation datasets. Use of the WT crystal structure to model anisotropic tumbling of G121V is justified since the available NMR data indicate no large-scale structural changes resulting from the mutation. First, large chemical shift differences resulting from the mutation are localized to regions immediately adjacent to the mutation site (Figure 2A). Second, the relationship between the predicted and experimental diffusion coefficients is similar, indicating a comparable rotational correlation time and degree of anisotropy (Supporting Information Figure S2). The final overall diffusion parameters calculated from the model-free results confirm that the structures are very similar (Supporting Information Table S2). Third, it has been shown that only modest changes in the circular dichroism spectra of G121V are observed, and the thermodynamics of urea and thermal denaturation are similar.[31] Finally, the backbone conformations of Gly121 in the available x-ray structures of the WT E:FOL and E:FOL:$NADP^+$ complex are in the region of conformational space that is allowed for valine, suggesting that a valine substitution can be accommodated without significant change in backbone conformation.

Model-free analysis of the ^{15}N relaxation data (Figure 3) shows that backbone amide and tryptophan imino motions in the WT and G121V E:FOL complexes are similar. In both complexes, select residues in the Met20 loop (residues 16–20), the adenosine binding loop (residues 67–69), and the hinge region (residue 88) have lower than average S^2 and nanosecond τ_e. Not surprisingly, the largest differences in dynamics between WT and G121V occur near the site of mutation in the FG loop (residues 119–123), where the substitution of the bulky valine results in an increase in S^2 and the introduction of R_{ex} terms. The average backbone S^2 values of residues 120 and 122 increase from 0.64 to 0.75 upon mutation, while S^2 for residue 121 increases from 0.47 (Gly121) to 0.65 (Val121). Motions of residues 120–123 that are on the order of 0.7 to 1.8 ns in the WT complex are on the picosecond time scale in G121V (40–50 ps). Thus, substitution of Gly121 by Val causes a decrease in the amplitude of backbone motions in this part of the FG loop and a shift to a faster timescale. The G121V substitution also affects the backbone dynamics of Met20 loop residues, with significant increases in S^2 for residues 11, 15, 17 and 18 (Figure 3).

Interestingly, there are also changes in the backbone amide relaxation of Gln65 and Thr68, located in the CD loop more than 25 Å from the site of the mutation. Gln65 in G121V shows a decrease in S^2 and new nanosecond timescale motions (Figure 3). The locations of these changes are shown on the structure of DHFR in Figure 4. In contrast, the backbone S^2 for Thr68 is increased slightly in the mutant. The occurrence of long-range communication between the active site loops in the major subdomain and the CD loop has been suggested previously on the basis of both experimental[81] and theoretical studies.[82,83]

Side-chain methyl ^2H relaxation in the G121V E:FOL complex

Methyl ^2H relaxation rates of $^{13}C^1H_2$ ^2H methyl groups of the E:FOL complex were measured at ^1H spectrometer frequencies of 600 and 800 MHz. Methyl model-free parameters (S^2_{axis}, τ_e) were determined by simultaneously fitting the ^2H quadrupolar relaxation at both magnetic fields (Figure 5) and were compared with parameters reported previously for the E:FOL complex of the WT enzyme (Figure 5B).[84] A complete set of the calculated methyl model-free parameters is shown in Supplementary Table S4.

The changes in methyl S^2_{axis} upon mutation to G121V are consistent with the changes in backbone S^2 (Figures 3 and 4). Locations of changes in S^2_{axis} between mutant and WT are

shown on the DHFR structure in Figure 6. Most notable are increases in S^2_{axis} at Ala117-β in the FG loop and Ala19-β and Met20-ε in the Met20 loop in G121V DHFR. Smaller increases in S^2_{axis} are observed for Val119-γ1/γ2 and Thr123-γ2 in the FG loop. Large increases in S^2_{axis} also occur for Leu110-δ1/δ2 and Leu112-δ1/δ2 located in β-strand F at the center of the major subdomain β-sheet. These methyl groups are packed tightly against each other and against the aromatic ring of Phe125 in the C-terminal portion of the FG loop. The introduction of valine at site 121 provides two additional methyl probes in G121V. The Val121 methyls exhibit significantly lower S^2_{axis} values (0.26, 0.28) than the average for valine (average S^2_{axis} of 0.71), but similar to that of Val119 (0.32, 0.33), also in the central portion of the FG loop. Low values of S^2_{axis} for Val119-γ1/γ2 and Val121-γ1/γ2 of G121V DHFR indicate that, although the amplitude of motions are diminished relative to WT, the FG loop remains flexible relative to the rest of the protein.

Backbone μs-ms timescale dynamics of G121V complexes

As the backbone μs-ms timescale dynamics of WT DHFR are very dependent on the nature of the bound ligands,[45,77] we used ^{15}N R_2 relaxation dispersion to study four complexes of G121V including E:FOL, E:FOL:$NADP^+$, E:THF:$NADP^+$ and E:THF:NADPH. The WT E:FOL:$NADP^+$ complex has been previously used to model the reactive Michaelis complex (E:DHF:NADPH) of DHFR.[25,29,43] The E:FOL complex can serve as a model for either the substrate binary (E:DHF) or product binary (E:THF) complex, although there are some notable changes in the WT backbone μs-ms timescale dynamics in the active-site loops between these complexes.[77] Altogether, these complexes represent four of the five major intermediates in the catalytic cycles of WT[24] and G121V DHFR.[34] The fifth complex, the holoenzyme (E:NADPH), is conformationally heterogeneous in the G121V complex, containing at least three different conformations,[29] and as such, was not investigated further due to the complexity of its spectra. A summary of the data, including fits, for those residues exhibiting relaxation dispersion, is shown in Figure S3.

R_2 relaxation dispersion spectroscopy monitors conformational exchange events on the μs-ms time scale. For two-site exchange between states A and B, the magnitude of the exchange contribution to R_2 (R_{ex}) depends on the rate of exchange ($k_{ex} = k_{AB} + k_{BA}$), the populations of the states (p_A and p_B), and the chemical shift difference between them ($\Delta\omega$).[85] A major advantage of R_2 relaxation dispersion techniques is the ability to characterize minor populations comprising <5% of the conformational ensemble that are `invisible' to other structural techniques.[86]

^{15}N R_2 relaxation dispersion for G121V E:FOL

Residues in the WT and G121V E:FOL complexes that exhibit ^{15}N relaxation dispersion are shown in Figure 7A. For both the WT and mutant enzyme, conformational exchange is observed in the cofactor-binding cleft (green), the active-site loops (red), and the C-terminal associated region (blue). However, a major difference is observed in the folate-binding pocket (gold), where many residues exhibit conformational exchange processes in the G121V E:FOL complex but not in the WT complex (Figure 7A). For the WT enzyme, the dispersion data for residues in the active site loops and cofactor-binding site can be fit to a single exchange process with $k_{ex} = k_{AB} + k_{BA} = 537\ s^{-1}$ and $p_B = 0.03$ at 306 K.[77] Similar kinetics are observed for residues in the active site and substrate binding site of the G121V mutant ($k_{ex} = 635\ s^{-1}$ and $p_B = 0.017$; Table 1). However, attempts to fit dispersion curves for residues in the active site, substrate binding site, and cofactor binding site with a global k_{ex} and p_B were unsatisfactory. Inclusion of the cofactor site residues in the cluster fits resulted in a large decrease in k_{ex} and significantly worse fits (as indicated by χ^2) for many residues in the active site loops and substrate binding site. We attempted unsuccessfully to fit the cofactor binding site dispersion as a separate cluster but the data are of insufficient

quality and residues 63, 65, and 77 in the adenosine binding site appear to exhibit different kinetics from the other residues. Even though we were unable to obtain robust fits for these dispersion curves, our data suggest strongly that the G121V mutation has decoupled fluctuations in the cofactor site from those in the active site and has introduced new conformational fluctuations in the substrate binding pocket.

The relaxation dispersion observed for residues in the substrate binding site of the G121V E:FOL complex does not appear to reflect dissociation of folate. Based on the known dissociation constant, the free enzyme is estimated to have a population (0.01%), very much lower than the population of the higher energy substate (p_B ~ 1%) determined using R_2 relaxation dispersion. As for the corresponding WT complex, the Δω values for residues in the active site loops of the G121V E:FOL complex differ from those expected for occluded-closed conformational transitions, indicating that the active site fluctuations do not involve formation of a closed excited state.

^{15}N R_2 relaxation dispersion for G121V product ternary complexes

It is notable that, in comparison to the corresponding WT complexes, dispersion is relatively weak and limited to a small number of residues in both the E:THF:$NADP^+$ and E:THF:NADPH complexes of G121V. Conformational exchange is observed for the same residues in the Met20 loop and FG loop of both G121V complexes, suggesting that similar conformational transitions are involved (Figure 7C, D, Supporting Information Table S6). As for the mutant E:FOL complex, the pattern of residues displaying dispersion and the dynamic chemical shift differences (Δω) indicate clearly that these fluctuations do not involve transitions to a closed excited state. It should be noted that Met20 loop residues with measurable conformational exchange also show small, but significant, chemical shift differences between the WT and G121V complexes (Figure 2). Weak dispersion is observed for several residues near the N-termini of the αC and αF helices, at the site of binding of the pyrophosphate moiety of the cofactor, in both the E:THF:$NADP^+$ and E:THF:NADPH complexes of the G121V mutant. Conformational exchange is also observed in these regions in the WT E:THF:$NADP^+$ complex and extends into the adenosine-binding loop (Figure 7C).

The observed relaxation dispersion in G121V E:THF:NADPH differs markedly from that in the corresponding complex of the WT enzyme,[45] (Figure 7D). Conformational exchange in the mutant DHFR complex is limited to a small number of residues in the active site loops, in immediate proximity to the site of mutation, in the cofactor-binding site, and in the C-terminal associated region. In contrast, for the WT complex, conformational exchange occurs for many residues around the substrate/product binding site but not in the cofactor binding cleft (Figure 7D). Thus, the μs-ms timescale dynamics in the product ternary complexes differ significantly for the WT and G121V mutant enzyme; the dynamics are very similar in the E:THF:$NADP^+$ and E:THF:NADPH complexes of the G121V mutant whereas the corresponding complexes of the WT enzyme differ greatly in their μs-ms time scale motions.

^{15}N R_2 relaxation dispersion for G121V E:FOL:$NADP^+$

Many more residues show dispersive behavior in the G121V E:FOL:$NADP^+$ complex than in the product ternary complexes of the mutant enzyme (Figure 7B). These include a large number of residues in the active-site loops, many of which also show dispersion in the WT E:FOL:$NADP^+$ complex (e.g. Asn18, Ala19, Met20, Trp22, Asn23, Gly96, Glu118, Val119, Glu120, Asp122, His149) where they report on a `closed-occluded' conformational change.[43,87] However, for the G121V E:FOL:$NADP^+$ complex, there is no correlation between the dynamic chemical shifts (Δω) determined from R_2 relaxation dispersion and the

equilibrium chemical shift difference ($\Delta\delta$) between closed and occluded conformations (Supporting Information Figure S4), showing that the μs-ms timescale dynamics in the occluded active-site loops of the mutant complex do not lead to sampling of the closed state.

Although the Gibbs free energy differences between higher and lower energy substates are similar for the WT E:FOL:$NADP^+$, WT E:THF:$NADP^+$ and G121V E:FOL:$NADP^+$ complexes, the enthalpy and entropy contributions differ significantly for the G121V E:FOL:$NADP^+$ complex (Table 2, Figure 8). Again, this indicates that the higher energy conformation is not closed. It is interesting to note, however, that the energy barriers ($\Delta G^‡$, $\Delta H^‡$, $T\Delta S^‡$) associated with the μs-ms timescale dynamics are similar among all three complexes (Table 2, Figure 8).

μs-ms timescale dynamics in the C-terminal associated region

All WT and G121V complexes show conformational exchange in the C-terminal associated region (residues 129–134, 155–159). The C-terminal associated region appears to sample similar higher energy conformational substates in all complexes, since $\Delta\omega$ values are similar for all WT and mutant enzyme complexes (Supporting Information Table S6). However, it should be noted that the nature of the bound ligand(s) and the identity of the amino acid at position 121 influence the kinetics and thermodynamics of the fluctuations in this region (Tables 1, 2). Neither the importance of the C-terminal dynamics, nor the impact of ligand-binding and/or mutagenesis on the motions in this region are yet understood.

Discussion

E. coli DHFR has been widely used as a model system to investigate the relationship between protein dynamics and enzyme catalysis.[23] One key finding has been that mutations distant from the active-site center can significantly impact rates of hydride transfer.[26–28,35,88,89] This behavior is consistent with the suggestion that there is a catalytically-important network of coupled protein motion extending from the enzyme surface into the active-site.[9,19–21] A key residue in this network is Gly121, which resides in the FG loop and is more than 15 Å from the active-site center. To obtain further insights into the roles of Gly121 and protein motion in DHFR, we used NMR relaxation techniques to measure protein dynamics over the ps to ms timescales for complexes representing intermediates in the catalytic cycle of G121V DHFR.

Structural models indicate that the G121V substitution can be accommodated in the occluded state with only minor conformational adjustment. In contrast, incorporation of the bulky valine side chain would result in major steric clashes in the closed or open states that would necessitate substantial rearrangement of the Met20 and GH loop conformations and the packing interactions between them. Further, simulations suggest that substitution of valine at position 121 leads to Met20 loop conformations that differ substantially from the closed form, and that a hydrogen bond between the Asp122 amide and Gly15 carbonyl, which helps stabilize the closed state, is disupted.[90,91] The predicted destabilization of the closed state is supported by NMR data for the E:FOL:$NADP^+$ and E:FOL:NADPH complexes, which are in the fully closed conformation in the WT enzyme but adopt the occluded conformation in the corresponding complexes of the G121V mutant.[29] The G121V E:NADPH complex, which is closed for WT DHFR, is predominantly occluded but with a minor population of a closed state present in slow exchange[29]; addition of the inhibitor methotrexate (MTX) to form the E:NADPH:MTX ternary complex drives the G121V mutant into a fully closed state.[92]

ps-ns timescale dynamics in G121V DHFR

In the WT enzyme, ps-ns timescale motions of DHFR are determined primarily by the overall backbone conformation (closed or occluded),[42,77] and we therefore used the E:FOL complex to probe ps-ns timescale dynamics in the occluded conformations of G121V DHFR; all of the G121V complexes studied here, representing four of the intermediates of the catalytic cycle, are in the occluded conformation.

The ps-ns timescale backbone and methyl side-chain dynamics are overall quite similar for the WT and G121V E:FOL complexes, with the largest differences in S^2 and τ_e occurring at the site of mutation (Figures 3 and 4). The Val substitution decreases the amplitude (increased S^2) and changes the timescale (decreased τ_e) of the backbone motions of residues 120–123 in the FG loop (Figure 3). These changes in FG loop dynamics are transmitted to both local and distant sites in the protein.

We first consider changes in side chain dynamics resulting from the incorporation of the bulky valine side chain. A decrease in the amplitude of side chain motions is observed for side chains in the FG loop that directly contact the side chain of Val 121(Val119 and Thr123). The motional changes are transmitted to the Ala19 and the Met20 methyl groups in the Met20 loop, more than 8 Å from the site of mutation, as well as the Ala117 methyl and Ile115 δ1 methyl group at the beginning of the FG loop (Figure 6). The relaxation experiments thus reveal a general restriction of side chain motion in the Met20 and FG loops due to the Val substitution and provide direct evidence for motional coupling between these regions of the protein. Our results are fully consistent with molecular dynamics simulations that revealed dynamic coupling between the Met20 and FG loops that is modulated by ligands and perturbed by the G121V substitution.[36,83] Importantly, however, the perturbations of DHFR dynamics extend far beyond the Met20/FG loop interface to distant regions of the protein. Observed changes in methyl order parameters reveal a pathway by which dynamic perturbations can be communicated 25–30 Å across the protein molecule from the site of the G121V mutation (Figure 6). The motional changes propagate outwards from the mutation site along the β-sheet, with restriction of the amplitude of side chain methyl groups of Leu8, Leu112, and Leu110 and of the Nε of Trp133. These residues are all in van der Waals contact and lie on one face of the β-sheet, packed against the aromatic ring of Phe125 which likely couples their motions to those of the FG loop. The side chain motional restrictions propagate further down strand βA to Leu4 and Ile2, then into the adenosine binding subdomain where increased order parameters are observed for Ile82 and Ala81 in the αE helix and Val88 in the EF loop. There is also a substantial decrease in S^2 for the Nε of Trp74 in the CD loop, close to the adenosine binding site. The changes in dynamics also extend, via Ile5 and Trp33, into the folate binding site.

The motional perturbations observed in the side chains are reflected in changes in ps-ns timescale backbone dynamics. Although there is a decrease in the amplitude of backbone motions for residues 120–122 (average increase in $S^2 = 0.14$), the FG loop remains relatively flexible (Figure 3). Restriction of backbone dynamics is also observed for Asp11, Gly15, Glu17, and Asn18 in the Met20 loop, providing further evidence that the motions of the FG and Met20 loops are coupled.

The largest increase in backbone S^2 in the Met20 loop is seen for Glu17, which undergoes the largest structural changes between the occluded and closed conformations (the heavy atom RMSD between Glu17 in the occluded and closed loop conformations is 11.0 Å). The shortest distance between Glu17 and any FG loop residue in the crystallographically observed occluded conformation is more than 9 Å. However, given the high flexibility of the Met20 and FG loops, it seems likely that conformational sampling would bring these loops into transient contact. The importance of contacts between the FG and Met20 loop has been

highlighted by mutational studies in which Asp122 is replaced by amino acids with side-chains of decreasing ability to hydrogen bond.[27]

The G121V mutation perturbs ps-ns time scale backbone dynamics far beyond the Met20 loop, in regions of the protein that are more than 25 Å distant from the site of mutation. The extent of these perturbations is seen clearly in Figure 4B, which maps residues that show changes in the amplitude (S^2) and/or time scale (τ_e) of backbone motions onto the DHFR structure. It seems likely that these dynamic perturbations are propagated through the network of dynamically coupled side chains that lie on one face of the β-sheet at the core of the loop subdomain and are then transmitted to the adenosine binding subdomain via contacts between the N-terminal region of strand βA and helix αE or are communicated via the bound folate ligand. For the majority of residues for which changes in ps-ns dynamics are observed, the backbone motions become more restricted (larger S^2) in the G121V mutant. However, for a subset of residues at the C-terminal end of the FG loop, the C-terminus, and at Gln65 (also the nearby side chain of Trp74) in the adenosine binding domain, the mutation increases the amplitude of the motions but shifts them to a slower time scale (Figure 4). Changes in backbone and side chain methyl group dynamics in the adenosine binding domain arising from mutation of Gly 121 to Val have also been reported for the complex of DHFR with NADPH and the drug methotrexate (MTX).[92] The NMR experiments thus provide insights into the molecular mechanism by which substitutions at Gly67 and Gly121 interact over long distances to exert non-additive effects on the catalytic activity of DHFR.[33]

Mechanism of allosteric communication to distant sites

DHFR exhibits allosteric bevavior in several ways. Binding of ligand in the substrate binding site alters the affinity for cofactor binding and *vice versa*.[24] Mutation of residues distant from the active site affects both binding affinity and hydride transfer kinetics and non-additive effects of double mutations provide evidence for coupled interaction networks spanning large distances within the protein.[33,35] The FG loop is connected to the active site via an evolutionarily conserved network of amino acids; insertion of a light senstive LOV2 domain into DHFR between residues 120 and 121 results in weak light-dependent allosteric control of DHFR activity.[12,93]

The present experiments show clearly that long-range structural changes are not a prerequisite for transmission of allosteric signals through a protein, but that perturbations associated with a local event can be propagated by dynamic changes, i.e. by changes in the conformational space available for sampling through thermal fluctuations of backbone or side chains. Figure 2A shows that the G121V mutation in the E:FOL complex leads to very few changes in backbone ^{1}H and ^{15}N chemical shifts, all of which are entirely localized to backbone amides lying within 9 Å of the site of mutation, in the FG loop itself and in the tightly coupled Met20 loop (Figure 2A). The G121V mutant adopts an occluded conformation that is extremely close to that of the WT complex; however, the mutation leads to substantial changes in dynamics, restricting the amplitude and changing the time scale of motions of residues in the FG loop and in the neighboring Met20 loop. The effects of the mutation are transmitted to distant sites not through propagation of structural change, as evidenced by the almost complete absence of changes in chemical shifts for residues outside the site of mutation, but through subtle changes in the accessible conformational space sampled by molecular fluctuations on the ps-ns time scale. Our results are fully consistent with theoretical approaches that suggest long-range allostery in DHFR arises from a redistribution of the conformational ensemble, with significant contributions from perturbations of the protein dynamics.[82]

μs-ms timescale dynamics in G121V DHFR

In contrast to ps-ns timescale dynamics of DHFR, the slower μs-ms timescale conformational fluctuations change significantly depending on the ligands that are bound to the enzyme.[45,77] It was therefore necessary to measure protein dynamics of several G121V complexes in order to elucidate the effect of mutation on these slower timescale dynamics.

The μs-ms timescale dynamics are quite similar for the FOL complexes of the WT and G121V protein, except in the substrate binding site (Figure 7A). Both exhibit extensive conformational fluctuations in the Met20 and FG loops, although the Δω values for corresponding residues differ suggesting that the WT and mutant proteins sample somewhat different conformational substates. Many residues in the cofactor binding site of the G121V E:FOL complex experience μs-ms timescale fluctuations although the current data are of insufficient quality to quantitate this process. Fluctuations in the cofactor site were observed previously for WT E:THF[45] and E:FOL[77] complexes and, on the basis of chemical shift correlations, we have suggested[45] a conformational selection mechanism of ligand binding. There are two significant differences in dynamics between the WT and G121V E:FOL complexes: the μs-ms timescale fluctuations in the active site loops propagate into the substrate binding site of the mutant enzyme but not WT, and the mutation appears to decouple the fluctuations in the cofactor binding site from the active site motions, as was previously observed for WT E:FOL:$NADP^+$.[94] As for the ps-ns timescale motions, the effects of the mutation are manifest in changes in μs-ms timescale dynamics in distant regions of the protein structure. Similar observations have been made for other enzymes; mutations in cyclophilin A and triosephosphate isomerase, for example, also result in perturbation of ms timescale fluctuations at distant sites.[95,96]

There are large differences in the μs-ms timescale dynamics between the product ternary complexes of the WT and G121V mutant enzyme. In the WT E:THF:$NADP^+$ complex, we observe four regions of conformational exchange – in the active-site loops, in the cofactor-binding cleft, for several residues in proximity to the p-aminobenzoic acid moiety of the product THF, and in the C-terminal associated region.[94] These fluctuations are mostly impaired in the corresponding complex of the mutant, most notably in the product and cofactor binding sites (Figure 7C). In the WT E:THF:$NADP^+$ complex, there are widespread fluctuations in all three active-site loops (Met20, FG and GH), reflecting conformational exchange between closed and occluded conformations of DHFR.[94] In contrast, very few residues in the Met20 and FG loops, all of which are in the immediate vicinity of the site of mutation, experience exchange processes in the G121V E:THF:$NADP^+$ complex. The Δω values for these residues do not reflect transitions into a closed conformational state. Thus, the active site region in the E:THF:$NADP^+$ complex of G121V fluctuates into an alternate conformational substate that differs from the closed state formed by the WT enzyme. In the C-terminal associated region, comparable μs-ms timescale dynamics are observed for WT and the G121V E:THF:$NADP^+$ complex, although there are small changes in the kinetics and thermodynamics (Table 1).

A very similar group of residues, located in the cofactor pyrophosphate binding site and in the immediate vicinity of the mutation site, exhibits μs-ms fluctuations in both the E:THF:NADPH and E:THF:$NADP^+$ complexes of the G121V enzyme (Figures 7C and D). Conformational exchange in the WT E:THF:NADPH complex is far more widespread than in the G121V mutant, with many residues in the Met20, FG, and GH loops exhibiting relaxation dispersion[45] (Figure 7D). Most importantly, numerous residues in the THF binding site undergo conformational fluctuations in the WT E:THF:NADPH complex that are completely abrogated in the G121V mutant. We have previously proposed that conformational fluctuations in the substrate/product binding pocket of the WT E:THF:NADPH complex play a key role in the release of product, since the rate of lower to

higher energy substate conversion (k_{AB} = 12 – 18 s^{-1}) is very similar to the THF dissociation rate constant (k_{off} = 13 s^{-1}).[45] The loss of these fluctuations in the G121V E:THF:NADPH complex is consistent with the decreased dissociation rate constant for THF for the mutant enzyme (k_{off} = 1.9 s^{-1}),[34] which is too slow to give measurable R_2 relaxation dispersion. Instead, for the G121V E:THF:NADPH complex, we observe μs-ms timescale dynamics in the αC helix, which forms the binding site for the ribose phosphate region of the cofactor. The structural fluctuations in the cofactor binding cleft of the G121V E:THF:NADPH complex, which we cannot detect in the corresponding WT complex using R_2 relaxation dispersion,[45] may also explain why the dissociation rate constant of NADPH is three times higher in the G121V protein compared to the WT enzyme.[34]

As noted above, the μs-ms timescale dynamics of the product ternary complexes (E:THF:$NADP^+$ and E:THF:NADPH) are similar for the G121V mutant but differ for the WT enzyme. We have shown elsewhere[45,77] that the conformational fluctuations in the active-site loops for the ternary product complexes of the WT enzyme allow the nicotinamide ring to transiently enter the active-site pocket. The different charge and/or shape of the reduced and oxidized forms of the ring leads to different dynamic behavior in the substrate and cofactor binding pockets for the E:THF:NADPH and E:THF:$NADP^+$ complexes of the WT protein.[45,77] Since we cannot detect similar active-site loop motions in the G121V complexes, it appears that, on the time scale of R_2 relaxation dispersion, the nicotinamide ring cannot transiently enter the active-site to affect dynamics in the substrate and cofactor binding sites. These findings suggest that the G121V mutation has uncoupled the active-site loop motions and the concomitant motion of the nicotinamide ring into the active-site from structural fluctuations in the binding pockets for cofactor and substrate/product. Structural fluctuations in the substrate/product binding pocket still depend on the motions of the active-site loops and the nicotinamide ring, whereas those in the cofactor binding site are now independent.

Perhaps the most relevant complex to elucidate the role of Gly121 in DHFR-catalyzed hydride transfer is the G121V E:FOL:$NADP^+$ complex. It has been suggested that the E:FOL:$NADP^+$ complex serves as a good model for the reactive E:DHF:NADPH (Michaelis) complex.[25,29,43] The E:FOL:$NADP^+$ complex of the WT enzyme adopts a closed ground state conformation that allows for close association between the pterin and nicotinamide rings. However, the G121V E:FOL:$NADP^+$ complex is clearly not in the closed conformation. Moreover, there is no experimental evidence from the R_2 relaxation dispersion experiments that the G121V complex even samples the closed conformation in thermally accessible higher energy states. Our results suggest that if the G121V E:FOL:$NADP^+$ complex does fluctuate from its occluded ground state into a closed conformation, either the kinetics of conformational exchange are too slow (i.e. k_{ex} < 100 s^{-1}) and/or the population of the closed conformation is too small (i.e. p_B < 1%) to observe by R_2 relaxation dispersion. It should be noted that pre-steady state kinetic analysis of the G121V enzyme revealed an additional step, not observed for the WT enzyme, associated with a conformational change that precedes hydride transfer.[34] This process, with a rate constant of 3.5 s^{-1} (at 298 K), is too slow to be detected by R_2 relaxation dispersion. Thus, there are potentially two conformational changes in the G121V E:FOL:$NADP^+$ complex. The first conformational change involving several of the Met20, FG and GH loop residues, and which we can detect using R_2 relaxation dispersion (k ~ 25 s^{-1} at 303 K), may poise the enzyme for the second conformational change (k ~ 3.5 s^{-1}) to the closed, catalytically-competent state, with the nicotinamide ring bound in the active site. Although all of the intermediates from the catalytic cycle adopt the fully occluded conformation, G121V can be forced into the closed state by binding NADPH and the drug methotrexate.[92] Conformational fluctuations are observed in the Met20 and FG loops of the G121V

E:NADPH:MTX complex, but amide resonances are severely exchange broadened, precluding identification of the structure of the state involved in the exchange.

Our results clearly indicate that conformational sampling is different between WT and G121V DHFR and provide insights into the molecular basis for the changes in both ligand affinities and the hydride transfer rate. It is noteworthy that many of the residues identified as being part of the network of coupled promoting motions have different ps-ns and/or μs-ms timescale dynamics in the G121V and WT complexes, including residues Ile14, Gly15, Tyr100 and Asp122.[9] The side chains of several aliphatic residues in and around the active site become more rigid in G121V and this may also impair the coupled motional network that promotes catalysis. Overall, the changes in the dynamics of the enzyme upon mutation of Gly121 to Val provide compelling evidence for motional coupling between residue 121 and other residues in the network.

Our findings are also entirely consistent with the dynamic energy landscape view of enzyme catalysis.[45] Changes in the kinetics and thermodynamics of conformational exchange and/or the nature of the higher energy substates can lead to substantial changes to enzyme function. For the E:THF:NADPH complex, the lowest energy conformation is very similar for the WT and G121V enzymes and thus differences in ligand dissociation appear to depend on differences in conformational sampling. In the case of the model Michaelis complex E:FOL:$NADP^+$, the nature of both the ground state and higher energy substates can help explain the 200-fold reduction in hydride transfer rate in the G121V enzyme compared to the WT protein. Thus, both the ground state and higher energy conformations of DHFR participate in enzyme catalysis. Our studies demonstrate that functional changes upon mutation are not only dependent on structural changes in the lowest energy conformations, but they can also be propagated through changes in the higher energy conformations and/or overall protein dynamics. This suggests novel forms of dynamic allostery[7,14–18] and offers new dimensions for molecular evolution.[97,98]

Supplementary Material

Refer to Web version on PubMed Central for supplementary material.

Acknowledgments

We thank Linda Tennant and Euvel Manlapaz for technical support, and John Chung and Gerard Kroon for their help with the NMR experiments.

This work was supported by grant GM75995 from the National Institutes of Health and by the Skaggs Institute for Chemical Biology. D.D.B. acknowledges support from a Canadian Institutes of Health Research (CIHR) postdoctoral fellowship.

Abbreviations

DHFR	dihydrofolate reductase
NMR	nuclear magnetic resonance
$NADP^+$	nicotinamide adenine dinucleotide phosphate
NADPH	reduced nicotinamide adenine dinucleotide phosphate
DHF	7,8-dihydrofolate
THF	5,6,7,8-tetrahydrofolate
MTX	methotrexate

CSA	chemical shift anisotropy
NOE	nuclear Overhauser effect
COPED	comparison of predicted and experimental diffusion tensors
RMSD	root mean square deviation

References

1. Zhou HX, Wlodek ST, McCammon JA. Conformation gating as a mechanism for enzyme specificity. Proc. Natl. Acad. Sci. USA. 1998; 95:9280–9283. [PubMed: 9689071]
2. Antoniou D, Caratzoulas S, Kalyanaraman C, Mincer JS, Schwartz SD. Barrier passage and protein dynamics in enzymatically catalyzed reactions. Eur. J. Biochem. 2002; 269:3103–3112. [PubMed: 12084050]
3. Benkovic SJ, Hammes-Schiffer S. A perspective on enzyme catalysis. Science. 2003; 301:1196–1202. [PubMed: 12947189]
4. Tousignant A, Pelletier JN. Protein motions promote catalysis. Chem. Biol. 2004; 11:1037–1042. [PubMed: 15324804]
5. Liang ZX, Klinman JP. Structural bases of hydrogen tunneling in enzymes: progress and puzzles. Curr. Opin. Struct. Biol. 2004; 14:648–655. [PubMed: 15582387]
6. Boehr DD, Dyson HJ, Wright PE. An NMR perspective on enzyme dynamics. Chem. Rev. 2006; 106:3055–3079. [PubMed: 16895318]
7. Goodey NM, Benkovic SJ. Allosteric regulation and catalysis emerge via a common route. Nat. Chem. Biol. 2008; 4:474–482. [PubMed: 18641628]
8. Benkovic SJ, Hammes GG, Hammes-Schiffer S. Free-Energy Landscape of Enzyme Catalysis. Biochemistry. 2008; 47:3317–3321. [PubMed: 18298083]
9. Agarwal PK, Billeter SR, Rajagopalan PTR, Benkovic SJ, Hammes-Schiffer S. Network of coupled promoting motions in enzyme catalysis. Proc. Natl. Acad. Sci. USA. 2002; 99:2794–2799. [PubMed: 11867722]
10. Tanikawa J, Nomura T, Macmillan EM, Shinagawa T, Jin W, Kokura K, Baba D, Shirakawa M, Gonda TJ, Ishii S. p53 suppresses c-Myb-induced trans-activation and transformation by recruiting the corepressor mSin3A. J. Biol. Chem. 2004; 279:55393–55400. [PubMed: 15509555]
11. Lockless SW, Ranganathan R. Evolutionarily conserved pathways of energetic connectivity in protein families. Science. 1999; 286:295–299. [PubMed: 10514373]
12. Reynolds KA, McLaughlin RN, Ranganathan R. Hot Spots for Allosteric Regulation on Protein Surfaces. Cell. 2011; 147:1564–1575. [PubMed: 22196731]
13. Dhulesia A, Gsponer J, Vendruscolo M. Mapping of Two Networks of Residues That Exhibit Structural and Dynamical Changes upon Binding in a PDZ Domain Protein. J. Am. Chem. Soc. 2008; 130:8931–8939. [PubMed: 18558679]
14. Cooper A, Dryden DT. Allostery without conformational change. A plausible model. Eur. Biophys. J. 1984; 11:103–109. [PubMed: 6544679]
15. Kern D, Zuiderweg ER. The role of dynamics in allosteric regulation. Curr. Opin. Struct. Biol. 2003; 13:748–757. [PubMed: 14675554]
16. Popovych N, Sun S, Ebright RH, Kalodimos CG. Dynamically driven protein allostery. Nat. Struct. Mol. Biol. 2006; 13:831–838. [PubMed: 16906160]
17. Swain JF, Gierasch LM. The changing landscape of protein allostery. Curr. Opin. Struct. Biol. 2006; 16:102–108. [PubMed: 16423525]
18. Tsai CJ, del Sol A, Nussinov R. Allostery: absence of a change in shape does not imply that allostery is not at play. J. Mol. Biol. 2008; 378:1–11. [PubMed: 18353365]
19. Sergi A, Watney JB, Wong KF, Hammes-Schiffer S. Freezing a single distal motion in dihydrofolate reductase. J. Phys. Chem. B Condens. Matter Mater. Surf. Interfaces. Biophys. 2006; 110:2435–2441. [PubMed: 16471835]

20. Watney JB, Agarwal PK, Hammes-Schiffer S. Effect of mutation on enzyme motion in dihydrofolate reductase. J. Am. Chem. Soc. 2003; 125:3745–3750. [PubMed: 12656604]
21. Wong KF, Selzer T, Benkovic SJ, Hammes-Schiffer S. Impact of distal mutations on the network of coupled motions correlated to hydride transfer in dihydrofolate reductase. Proc. Natl. Acad. Sci. USA. 2005; 102:6807–6812. [PubMed: 15811945]
22. Chen J, Dima RI, Thirumalai D. Allosteric Communication in Dihydrofolate Reductase: Signaling Network and Pathways for Closed to Occluded Transition and Back. J. Mol. Biol. 2007; 374:250–266. [PubMed: 17916364]
23. Schnell JR, Dyson HJ, Wright PE. Structure, dynamics and catalytic function of dihydrofolate reductase. Ann. Rev. Biophys. Biomol. Struct. 2004; 33:119–140. [PubMed: 15139807]
24. Fierke CA, Johnson KA, Benkovic SJ. Construction and evaluation of the kinetic scheme associated with dihydrofolate reductase from *Escherichia coli*. Biochemistry. 1987; 26:4085–4092. [PubMed: 3307916]
25. Sawaya MR, Kraut J. Loop and subdomain movements in the mechanism of *Escherichia coli* dihydrofolate reductase: crystallographic evidence. Biochemistry. 1997; 36:586–603. [PubMed: 9012674]
26. Miller GP, Benkovic SJ. Deletion of a highly motional residue affects formation of the Michaelis complex for *Escherichia coli* dihydrofolate reductase. Biochemistry. 1998; 37:6327–6335. [PubMed: 9572847]
27. Miller GP, Benkovic SJ. Strength of an interloop hydrogen bond determines the kinetic pathway in catalysis by *Escherichia coli* dihydrofolate reductase. Biochemistry. 1998; 37:6336–6342. [PubMed: 9572848]
28. Miller GP, Wahnon DC, Benkovic SJ. Interloop contacts modulate ligand cycling during catalysis by *Escherichia coli* dihydrofolate reductase. Biochemistry. 2001; 40:867–875. [PubMed: 11170407]
29. Venkitakrishnan RP, Zaborowski E, McElheny D, Benkovic SJ, Dyson HJ, Wright PE. Conformational changes in the active site loops of dihydrofolate reductase during the catalytic cycle. Biochemistry. 2004; 43:16046–16055. [PubMed: 15609999]
30. Antikainen NM, Smiley RD, Benkovic SJ, Hammes GG. Conformation coupled enzyme catalysis: single-molecule and transient kinetics investigation of dihydrofolate reductase. Biochemistry. 2005; 44:16835–16843. [PubMed: 16363797]
31. Gekko K, Kunori Y, Takeuchi H, Ichihara S, Kodama M. Point mutations at glycine-121 of *Escherichia coli* dihydrofolate reductase: Important roles of a flexible loop in the stability and function. J. Biochem. 1994; 116:34–41. [PubMed: 7798183]
32. Gekko K, Yamagami K, Kunori Y, Ichibara S, Kodama M, Iwakura M. Effects of point mutation in a flexible loop on the stability and enzymatic function of *Escherichia coli* dihydrofolate reductase. J. Biochem. 1993; 113:74–80. [PubMed: 8454578]
33. Ohmae E, Iriyama K, Ichihara S, Gekko K. Nonadditive effects of double mutations at the flexible loops, glycine-67 and glycine-121, of *Escherichia coli* dihydrofolate reductase on its stability and function. J. Biochem. 1998; 123:33–41. [PubMed: 9504406]
34. Cameron CE, Benkovic SJ. Evidence for a functional role of the dynamics of glycine-121 of *Escherichia coli* dihydrofolate reductase obtained from kinetic analysis of a site-directed mutant. Biochemistry. 1997; 36:15792–15800. [PubMed: 9398309]
35. Rajagopalan PT, Lutz S, Benkovic SJ. Coupling interactions of distal residues enhance dihydrofolate reductase catalysis: mutational effects on hydride transfer rates. Biochemistry. 2002; 41:12618–12628. [PubMed: 12379104]
36. Rod TH, Radkiewicz JL, Brooks CL. Correlated motion and the effect of distal mutations in dihydrofolate reductase. Proc. Natl. Acad. Sci. USA. 2003; 100:6980–6985. [PubMed: 12756296]
37. Sikorski RS, Wang L, Markham KA, Rajagopalan PT, Benkovic SJ, Kohen A. Tunneling and coupled motion in *Escherichia coli* dihydrofolate reductase catalysis. J. Am. Chem. Soc. 2004; 126:4778–4779. [PubMed: 15080672]
38. Wang L, Tharp S, Selzer T, Benkovic SJ, Kohen A. Effects of a distal mutation on active site chemistry. Biochemistry. 2006; 45:1383–1392. [PubMed: 16445280]

39. Wang L, Goodey NM, Benkovic SJ, Kohen A. The role of enzyme dynamics and tunnelling in catalysing hydride transfer: studies of distal mutants of dihydrofolate reductase. Philos. Trans. R. Soc. London B Biol. Sci. 2006; 361:1307–1315. [PubMed: 16873118]
40. Epstein DM, Benkovic SJ, Wright PE. Dynamics of the dihydrofolate reductase folate complex: Catalytic sites and regions known to undergo conformational change exhibit diverse dynamical features. Biochemistry. 1995; 34:11037–11048. [PubMed: 7669761]
41. Falzone CJ, Wright PE, Benkovic SJ. Dynamics of a flexible loop in dihydrofolate reductase from *Escherichia coli* and its implication for catalysis. Biochemistry. 1994; 33:439–442. [PubMed: 8286374]
42. Osborne MJ, Schnell J, Benkovic SJ, Dyson HJ, Wright PE. Backbone dynamics in dihydrofolate reductase complexes: Role of loop flexibility in the catalytic mechanism. Biochemistry. 2001; 40:9846–9859. [PubMed: 11502178]
43. McElheny D, Schnell JR, Lansing JC, Dyson HJ, Wright PE. Defining the role of active-site loop fluctuations in dihydrofolate reductase catalysis. Proc. Natl. Acad. Sci. USA. 2005; 102:5032–5037. [PubMed: 15795383]
44. Swinger KK, Rice PA. Structure-based Analysis of HU-DNA Binding. J. Mol. Biol. 2007; 365:1005–1016. [PubMed: 17097674]
45. Boehr DD, McElheny D, Dyson HJ, Wright PE. The dynamic energy landscape of dihydrofolate reductase catalysis. Science. 2006; 313:1638–1642. [PubMed: 16973882]
46. Swint-Kruse L, Fisher HF. Enzymatic reaction sequences as coupled multiple traces on a multidimensional landscape. Trends Biochem. Sci. 2008; 33:104–112. [PubMed: 18261912]
47. Grzesiek S, Bax A. Correlating backbone amide and side chain resonances in larger proteins by multiple relayed triple resonance NMR. J. Am. Chem. Soc. 1992; 114:6291–6293.
48. Wittekind M, Mueller L. HNCACB, a high-sensitivity 3D NMR experiment to correlate amide-proton and nitrogen resonances with the alpha- and beta-carbon resonances in proteins. J. Magn. Reson. 1993; 101:201–205.
49. Muhandiram DR, Kay LE. Gradient-enhanced triple-resonance three-dimensional NMR experiments with improved sensitivity. J. Magn. Reson. Series B. 1994; 103:203–216.
50. Yamazaki T, Lee W, Revington M, Mattiello DL, Dahlquist FW, Arrowsmith CH, Kay LE. An HNCA pulse scheme for the backbone assignment of ^{15}N, ^{13}C, ^{2}H-labeled Proteins: Application to a 37-kDa *Trp* repressor-DNA complex. J. Am. Chem. Soc. 1994; 116:6464–6465.
51. Kay LE, Ikura M, Bax A. Proton-proton correlation via carbon-carbon couplings: a three-dimensional NMR approach for the assignment of aliphatic resonances in proteins labeled with carbon-13. J. Am. Chem. Soc. 1990; 112:888–889.
52. Montelione GT, Lyons BA, Emerson SD, Tashiro M. An efficient triple resonance experiment using carbon-13 isotropic mixing for determining sequence-specific resonance assignments of isotopically-enriched proteins. J. Am. Chem. Soc. 1992; 114:10974–10975.
53. Farrow NA, Zhang O, Forman-Kay JD, Kay LE. Comparison of the backbone dynamics of a folded and an unfolded SH3 domain existing in solution in aqueous buffer. Biochemistry. 1995; 34:868–878. [PubMed: 7827045]
54. Jones JA, Hodgkinson P, Barker AL, Hore PJ. Optimal sampling strategies for the measurement of spin-spin relaxation times. J. Magn. Reson. 1996; 113:25–34.
55. Palmer AG, Cavanagh J, Wright PE, Rance M. Sensitivity improvement in proton-detected two-dimensional heteronuclear correlation NMR spectroscopy. J. Magn. Reson. 1991; 93:151–170.
56. Press, WH.; Teukolsky, SA.; Vetterling, WT.; Flannery, BP. Numerical Recipes in C. Cambridge University Press; Cambridge U.K.: 1992.
57. Markley JL, Horseley WJ, Klein MP. Spin-lattice relaxation in slowly relaxing complex spectra. J. Chem. Phys. 1971; 55:3604–3605.
58. Schurr JM, Babcock HP, Fujimoto BS. A test of the model-free formulas. Effects of anisotropic rotational diffusion and dimerization. J. Magn. Reson. B. 1994; 105:211–224. [PubMed: 7850167]
59. Osborne MJ, Wright PE. Anisotropic rotational diffusion in model-free analysis for a ternary-DHFR complex. J. Biomol. NMR. 2001; 19:209–230. [PubMed: 11330809]
60. Korzhnev DM, Orekhov VY, Arseniev AS. Model-free approach beyond the borders of its applicability. J. Magn. Reson. 1997; 127:184–191. [PubMed: 9281482]

61. Garcia de la Torre JG, Bloomfield VA. Hydrodynamic properties of complex, rigid, biological macromolecules: theory and applications. Q. Rev. Biophys. 1981; 14:81–139. [PubMed: 7025081]
62. Lee LK, Rance M, Chazin WJ, Palmer AG. Rotational diffusion anisotropy of proteins from simultaneous analysis of ^{15}N and ^{13}C alpha nuclear spin relaxation. J. Biomol. NMR. 1997; 9:287–298. [PubMed: 9204557]
63. Kroenke CD, Rance M, Palmer AG. Variability of the ^{15}N chemical shift anisotropy in *Escherichia coli* ribonuclease H in solution. J. Am. Chem. Soc. 1999; 121:10119–10125.
64. Case DA. Calculations of NMR dipolar coupling strengths in model peptides. J. Biomol. NMR. 1999; 15:95–102. [PubMed: 10605083]
65. Clore GM, Szabo A, Bax A, Kay LE, Driscoll PC, Gronenborn AM. Deviations from the simple two-parameter model-free approach to the interpretation of nitrogen-15 nuclear magnetic relaxation of proteins. J. Am. Chem. Soc. 1990; 112:4989–4991.
66. d'Auvergne EJ, Gooley PR. The use of model selection in the model-free analysis of protein dynamics. J. Biomol. NMR. 2003; 25:25–39. [PubMed: 12566997]
67. Chen J, Brooks CL, Wright PE. Model-free analysis of protein dynamics: assessment of accuracy and model selection protocols based on molecular dynamics simulations. J. Biomol. NMR. 2004; 29:243–257. [PubMed: 15213423]
68. Ebert MO, Bae SH, Dyson HJ, Wright PE. NMR relaxation study of the complex formed between CBP and the activation domain of the nuclear hormone receptor coactivator ACTR. Biochemistry. 2008; 47:1299–1308. [PubMed: 18177052]
69. Muhandiram DR, Yamazaki T, Sykes BD, Kay LE. Measurement of ^{2}H T_1 and $T_{1\rho}$ relaxation times in uniformly ^{13}C-labeled and fractionally ^{2}H-labeled proteins in solution. J. Am. Chem. Soc. 1995; 117:11536–11544.
70. Palmer AG, Rance M, Wright PE. Intramolecular motions of a zinc finger DNA-binding domain from Xfin characterized by proton-detected natural abundance ^{13}C NMR spectroscopy. J. Am. Chem. Soc. 1991; 113:4371–4380.
71. Viles JH, Duggan BM, Zaborowski E, Schwarzinger S, Huntley JJ, Kroon GJ, Dyson HJ, Wright PE. Potential bias in NMR relaxation data introduced by peak intensity analysis and curve fitting methods. J. Biomol. NMR. 2001; 21:1–9. [PubMed: 11693564]
72. Abragam, A. Principles of Nuclear Magnetism. Clarendon Press; Oxford: 1961.
73. Mittermaier A, Kay LE, Forman-Kay JD. Analysis of deuterium relaxation-derived methyl axis order parameters and correlation with local structure. J. Biomol. NMR. 1999; 13:181–185. [PubMed: 20700817]
74. Kay LE, Torchia DA, Bax A. Backbone dynamics of proteins as studied by ^{15}N inverse detected heteronuclear NMR spectroscopy: application to staphylococcal nuclease. Biochemistry. 1989; 28:8972–8979. [PubMed: 2690953]
75. Loria JP, Rance M, Palmer AG. A relaxation-compensated Carr-Purcell-Meiboom-Gill sequence for characterizing chemical exchange by NMR spectroscopy. J. Am. Chem. Soc. 1999; 121:2331–2332.
76. Skrynnikov NR, Dahlquist FW, Kay LE. Reconstructing NMR spectra of “invisible” excited protein states using HSQC and HMQC experiments. J. Am. Chem. Soc. 2002; 124:12352–12360. [PubMed: 12371879]
77. Boehr DD, McElheny D, Dyson HJ, Wright PE. Millisecond timescale fluctuations in dihydrofolate reductase are exquisitely sensitive to the bound ligands. Proc. Natl. Acad. Sci. USA. 2010; 107:1373–1378. [PubMed: 20080605]
78. Ferrage F, Cowburn D, Ghose R. Accurate sampling of high-frequency motions in proteins by steady-state (15)N-{(1)H} nuclear Overhauser effect measurements in the presence of cross-correlated relaxation. J. Am. Chem. Soc. 2009; 131:6048–6049. [PubMed: 19358609]
79. Lipari G, Szabo A. Model-free approach to the interpretation of nuclear magnetic resonance relaxation in macromolecules. 2. Analysis of experimental results. J. Am. Chem. Soc. 1982; 104:4559–4570.
80. Lipari G, Szabo A. Model-free approach to the interpretation of nuclear magnetic resonance relaxation in macromolecules. 1. Theory and range of validity. J. Am. Chem. Soc. 1982; 104:4546–4559.

81. Ohmae E, Iriyama K, Ichihara S, Gekko K. Effects of point mutations at the flexible loop glycine-67 of *Escherichia coli* dihydrofolate reductase on its stability and function. J. Biochem. 1996; 119:703–710. [PubMed: 8743572]
82. Pan H, Lee JC, Hilser VJ. Binding sites in *Escherichia coli* dihydrofolate reductase communicate by modulating the conformational ensemble. Proc. Natl. Acad. Sci. USA. 2000; 97:12020–12025. [PubMed: 11035796]
83. Radkiewicz JL, Brooks CL. Protein dynamics in enzymatic catalysis: Exploration of dihydrofolate reductase. J. Am. Chem. Soc. 2000; 122:225–231.
84. Schnell JR, Dyson HJ, Wright PE. Effect of cofactor binding and loop conformation on side chain methyl dynamics in dihydrofolate reductase. Biochemistry. 2004; 43:374–383. [PubMed: 14717591]
85. Palmer AG. Nmr probes of molecular dynamics: overview and comparison with other techniques. Annu. Rev. Biophys. Biomol. Struct. 2001; 30:129–155. [PubMed: 11340055]
86. Mittermaier A, Kay LE. New Tools Provide New Insights in NMR Studies of Protein Dynamics. Science. 2006; 312:224–228. [PubMed: 16614210]
87. Osborne MJ, Venkitakrishnan RP, Dyson HJ, Wright PE. Diagnostic chemical shift markers for loop conformation and cofactor binding in dihydrofolate reductase complexes. Protein Sci. 2003; 12:2230–2238. [PubMed: 14500880]
88. Adams J, Johnson K, Matthews R, Benkovic SJ. Effects of distal point-site mutations on the binding and catalysis of dihydrofolate reductase from *Escherichia coli*. Biochemistry. 1989; 28:6611–6618. [PubMed: 2675972]
89. Wagner CR, Huang Z, Singleton SF, Benkovic SJ. Molecular basis for nonadditive mutational effects in *Escherichia coli* dihydrofolate reductase. Biochemistry. 1995; 34:15671–15680. [PubMed: 7495797]
90. Thorpe IF, Brooks CL. Barriers to hydride transfer in wild type and mutant dihydrofolate reductase from E-coli. J. Phys. Chem. B. 2003; 107:14042–14051.
91. Thorpe IF, Brooks CL. The coupling of structural fluctuations to hydride transfer in dihydrofolate reductase. Proteins. 2004; 57:444–457. [PubMed: 15382243]
92. Mauldin RV, Sapienza PJ, Petit CM, Lee AL. Structure and dynamics of the G121V dihydrofolate reductase mutant: lessons from a transition-state inhibitor complex. PLoS. One. 2012; 7:e33252. [PubMed: 22428003]
93. Lee J, Natarajan M, Nashine VC, Socolich M, Vo T, Russ WP, Benkovic SJ, Ranganathan R. Surface sites for engineering allosteric control in proteins. Science. 2008; 322:438–442. [PubMed: 18927392]
94. Boehr DD, Dyson HJ, Wright PE. Conformational relaxation following hydride transfer plays a limiting role in dihydrofolate reductase catalysis. Biochemistry. 2008; 47:9227–9233. [PubMed: 18690714]
95. Eisenmesser EZ, Millet O, Labeikovsky W, Korzhnev DM, Wolf-Watz M, Bosco DA, Skalicky JJ, Kay LE, Kern D. Intrinsic dynamics of an enzyme underlies catalysis. Nature. 2005; 438:117–121. [PubMed: 16267559]
96. Wang Y, Berlow RB, Loria JP. Role of loop-loop interactions in coordinating motions and enzymatic function in triosephosphate isomerase. Biochemistry. 2009; 48:4548–4556. [PubMed: 19348462]
97. Ma BY, Wolfson HJ, Nussinov R. Protein functional epitopes: hot spots, dynamics and combinatorial libraries. Curr. Opin. Struct. Biol. 2001; 11:364–369. [PubMed: 11406388]
98. James LC, Tawfik DS. Conformational diversity and protein evolution--a 60-year-old hypothesis revisited. Trends Biochem. Sci. 2003; 28:361–368. [PubMed: 12878003]
99. Schrödinger, L. The PyMOL Molecular Graphics System. 2013.
100. Otting G. Experimental NMR techniques for studies of protein-ligand interactions. Curr. Opin. Struct. Biol. 1993; 3:760–768.

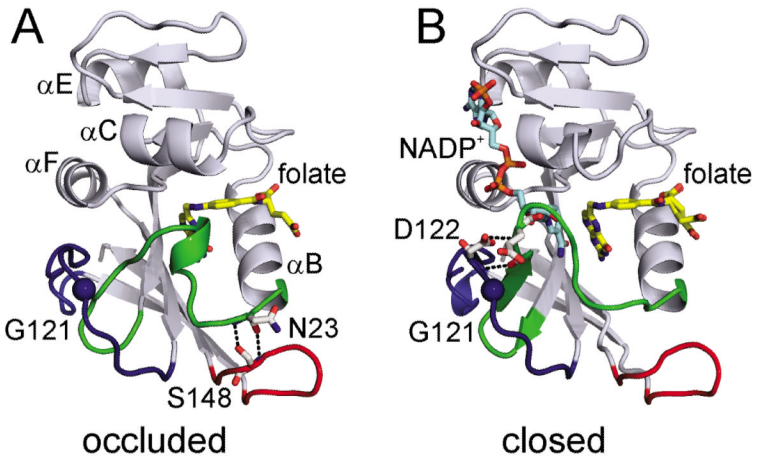

Figure 1.

Structures representing the (A) occluded (PDB 1RX7)[25] and (B) closed loop conformations (PDB 1RX2)[25] of *E. coli* DHFR. The active site loops are colored in green (Met20), blue (F–G), and red (G–H). Residues involved in hydrogen-bonding interactions between these loops are shown as sticks and labeled. Hydrogen bonds that stabilize the different loop conformations are indicated with dashed lines. In the occluded conformation of the Met20 loop (A), hydrogen bonds are formed between Asn23 in the F–G loop and Ser148 in the Met20 loop. In the closed conformation of the Met20 loop (B), hydrogen bonds are formed between Asp122 in the F–G loop and Gly15 and Glu17 in the Met20 loop. The figure was prepared using PyMOL.[99]

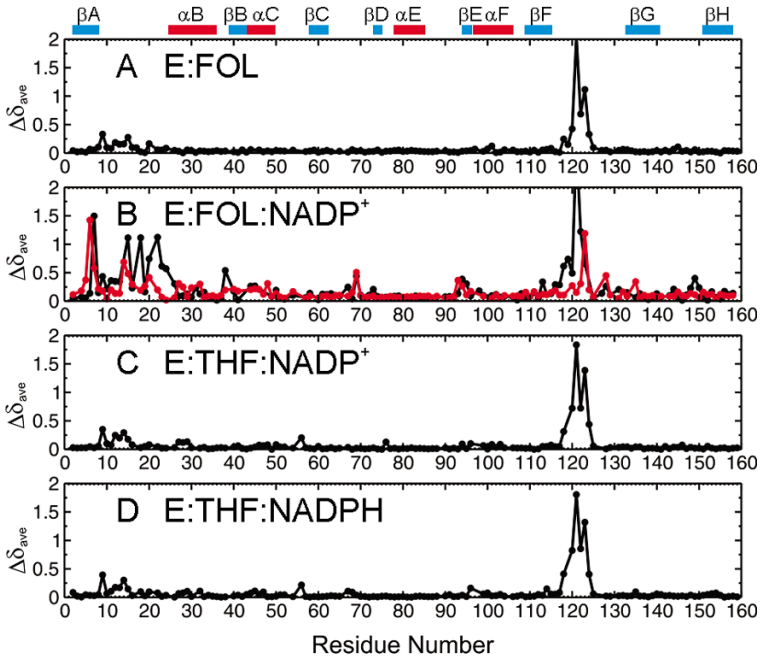

Figure 2.

Backbone amide $^{1}H^{N}$ and ^{15}N chemical shift differences between WT and G121V DHFR complexes, (A) E:FOL, (B) E:FOL:NADP$^+$, (C) E:THF:NADP$^+$ and (D) E:THF:NADPH. The weighted average shift difference ($\Delta\delta_{ave}$) for each residue was calculated as $((\Delta\delta_H)^2 + (\Delta\delta_N/5)^2)^{1/2}$ where $\Delta\delta_{H,N}$ is δ(G121V) – δ(WT).[100] For E:FOL:NADP$^+$ (B), the black line is a comparison between G121V E:FOL:NADP$^+$ and WT E:FOL:NADP$^+$ and the red line is a comparison between G121V E:FOL:NADP$^+$ and G121V E:THF:NADP$^+$.

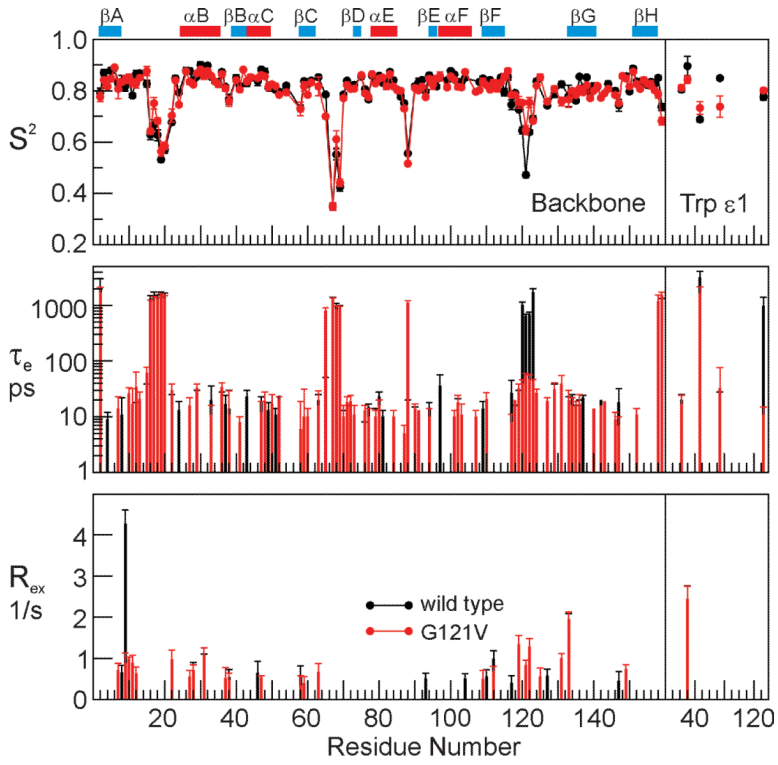

Figure 3.

Backbone amide and tryptophan imino model-free parameters S^2, τ_e and R_{ex} for the WT (black) and G121V (red) E:FOL complexes extracted from fits to data at 500 and 600 MHz. Values for R_{ex} are reported for 600 MHz.

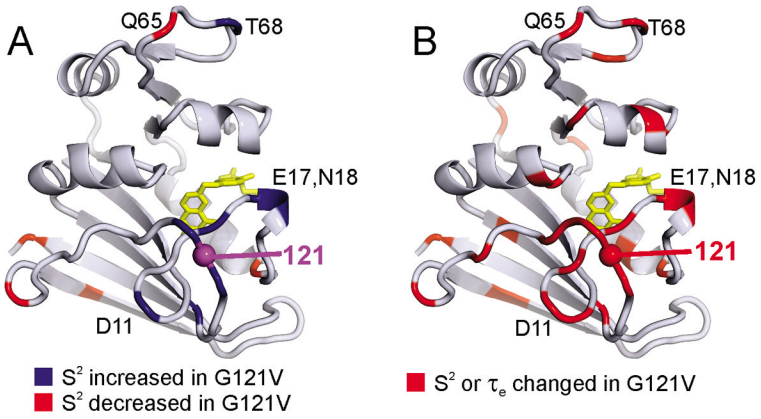

Figure 4.

Changes in dynamics in the G121V E:FOL complex, mapped onto the DHFR structure (PDB 1RX7)[25] A. Change in backbone amide S^2 between the WT and G121V E:FOL binary complexes. Blue, increase in S^2 showing restriction of ps-ns backbone motion in the mutant; red, decreased S^2, indicating increased amplitude of backbone motion in mutant. B. Location of residues that show changes in amplitude (S^2) and/or timescale (τ_e) of ps-ns backbone amide motions caused by the G121V mutation.

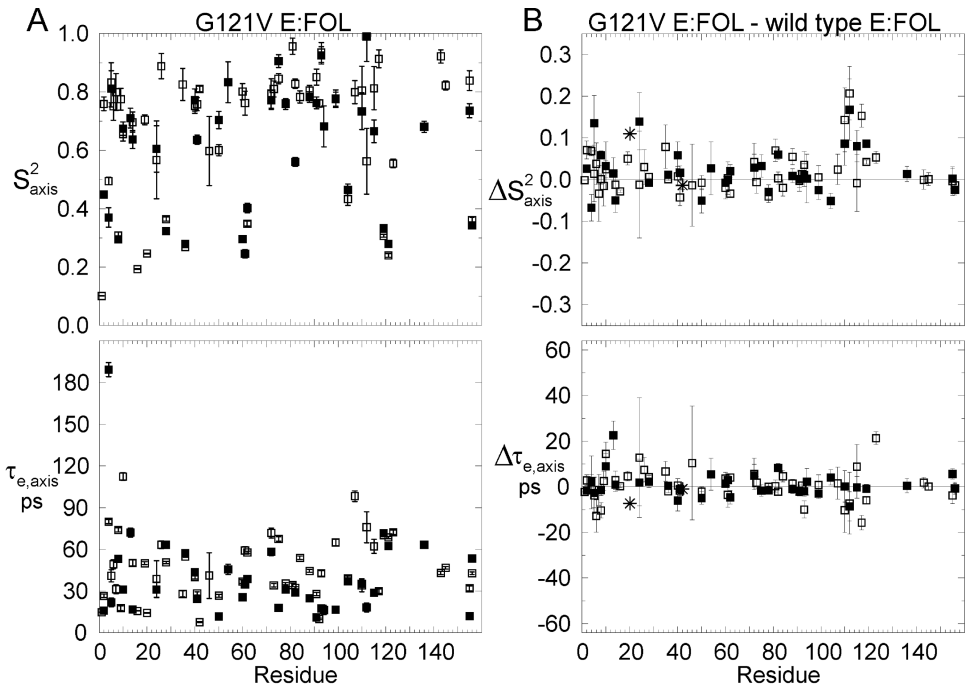

Figure 5.

Model-free parameters derived from methyl-incorporated deuterium relaxation data for the E:FOL complex of G121V DHFR. Shown are the methyl axis order parameters (S^2_{axis}) and internal correlation times (τ_e) for A the G121V E:FOL complex and B the deviations from WT behavior. Differences are shown as G121V minus WT. Model-free parameters were extracted from fits to R_1 (^{2}H) and $R_{1\rho}$ (^{2}H) at ^{1}H spectrometer frequencies of 600 and 800 MHz. Model-free parameters for the WT complex are from published work.[84] Parameters for Met20-ε and Met42-ε in WT DHFR were derived from 600 MHz (^{1}H frequency) spectra of a binary complex with dihydrofolate, used to resolve overlap in the spectra of the E:FOL complex.[84] Changes in dynamics for Met20 and Met42 are indicated with a star in B. Ala-β, Thr-γ2, Met-ε, Ile-γ2, Leu-δ1 and Val-γ1 are shown as open squares. Ile-δ1, Leu-δ2 and Val-γ2 are shown as filled squares.

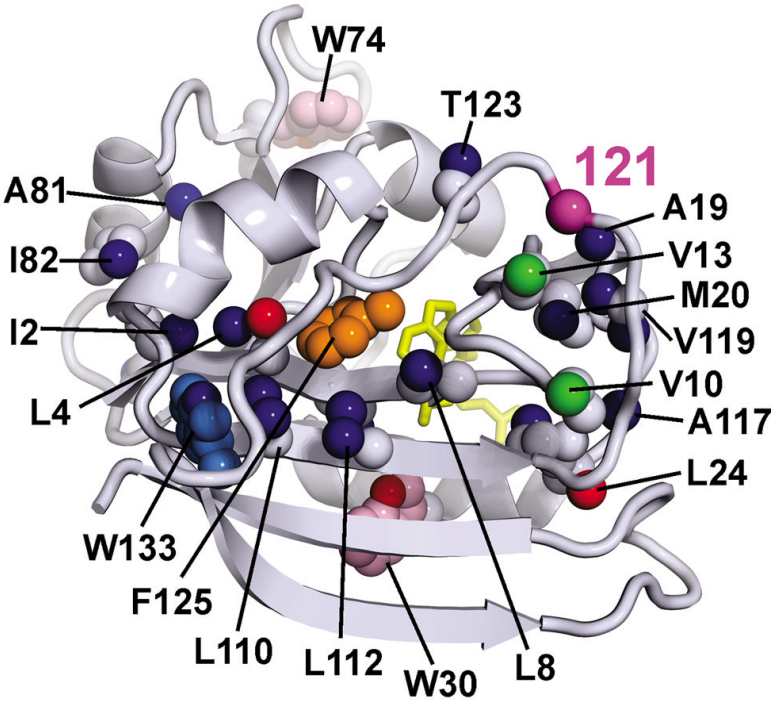

Figure 6.

Location of methyl groups that show altered S^2_{axis}. Blue, increased motional restriction (decreased amplitude/increased S^2_{axis}), red, increased motion (decreased S^2_{axis}), green, methyl groups that show slower time scale motion (larger τ_e) in the G121V mutant. Tryptophan side chains that show changes in Nε order parameters or τ_e are shown. Red Nε/pink side chain indicates increased flexibility, blue Ne/pale blue side chain indicates more restricted side chain dynamics in the mutant protein. The mutation site, Gly121, is indicated and folate is shown as yellow sticks. Selected sites in the backbone and side-chain are labeled. Figures were prepared using PyMol.[99]

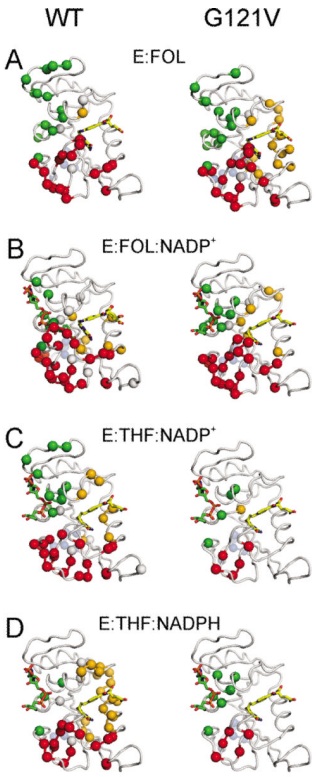

Figure 7.

Comparison of μs-ms timescale backbone dynamics between WT (left) and G121V (right) DHFR complexes (A) E:FOL, (B) E:FOL:$NADP^+$, (C) E:THF:$NADP^+$ and (D) E:THF:NADPH. Residues displaying conformational exchange (R_{ex}) are highlighted as colored spheres (red – Met20, FG and GH active-site loops, green – cofactor binding cleft, gold – substrate/product binding site, grey – other residues, pale blue (at the back of each structure) – C-terminal associated region). The coordinates used are 1RX7 (WT and G121V E:FOL), 3QL3/1RX2 (WT E:FOL:$NADP^+$, a closed conformation). For everything else the coordinate set 1RX6 (the 5, 10 dideazatetrahydrofolate (ddTHF)-NADPH complex) was used to model an occluded conformation with the adenosine ring bound but with the nicotinamide disordered and solvent-exposed outside the active site. Substrate molecules (ddTHF, FOL) are shown as yellow sticks, cofactors ($NADP^+$, NADPH are shown as green and red (phosphate) sticks).

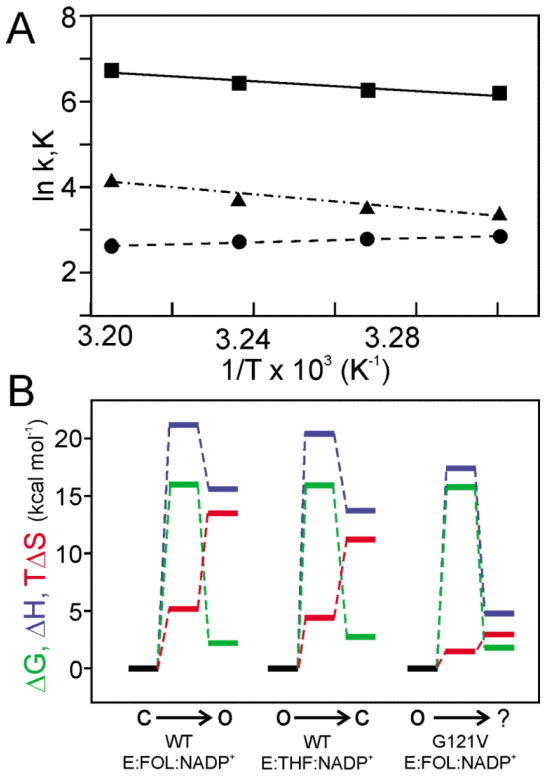

Figure 8.

A. Temperature dependence of the conformational exchange kinetics in the G121V E:FOL:NADP$^+$ complex for the active-site region. Rate constants for the transitions from the excited state to the ground state [k_{BA} (■)] and from the ground state to the excited state [k_{AB} (▲)] and the equilibrium constant [k_{BA}/k_{AB} (●)] are plotted. B. Thermodynamic comparison of the G121V E:FOL:NADP$^+$ complex (occluded ground state, unknown excited state; o → ?) with WT E:FOL:NADP$^+$ (closed ground state, occluded excited state; c → o) and WT E:THF:NADP$^+$ (occluded ground state, closed excited state; o → c) dynamics at 298 K. Thermodynamic barriers were calculated using transition-state theory according to Materials and Methods. ΔG, ΔH and TΔS traces are colored green, blue and red respectively.

Table 1

Kinetic and thermodynamic fitting parameters for WT and G121V DHFR ^{15}N R_2 relaxation dispersion curves

	WT[a,b]						**G121V**[a]					
	Cluster 1, active site[c]			**Cluster 2, C-term region**			**Cluster 1, active site**[c]			**Cluster 2, C-term region**		
	p_b	**$k_{AB}(s^{-1})$**	**k_{BA} (s^{-1})**	**p_b**	**$k_{AB}(s^{-1})$**	**k_{BA} (s^{-1})**	**p_b**	**$k_{AB}(s^{-1})$**	**k_{BA} (s^{-1})**	**p_b**	**$k_{AB}(s^{-1})$**	**k_{BA} (s^{-1})**
E:F												
306 K	0.030	16.1	521	0.031	14.9	465	0.017[d]	11.0	624	0.034	46.8	1320
E:F:N$^+$												
303 K	0.043	20.4	457	0.038	37.8	972	0.055	28.1	484	0.032	29.8	900
306 K	0.055	30.5	524	0.037	45.1	1234	0.060	32.8	517	0.036	32.8	871
309 K	0.072	43.0	552	n.d.[e]	n.d.[e]	n.d.[e]	0.062	40.0	605	n.d.[e]	n.d.[e]	n.d.[e]
312 K	0.082	53.2	598	n.d.[e]	n.d.[e]	n.d.[e]	0.069	61.5	833	n.d.[e]	n.d.[e]	n.d.[e]
E:T:N$^+$												
300 K	0.014[f] (0.030)	18.5[f] (50.8)	1280[f] (1650)	0.022	12.4	538	0.069	47.6	644	0.024	17.2	714
E:T:NH												
300 K	0.025	18.5	734	0.018	11.4	610	n.d.[g]	n.d.[g]	n.d.[g]	n.d.[g]	n.d.[g]	n.d.[g]
305 K	n.d.[g]	n.d.[g]	n.d.[g]	n.d.[g]	n.d.[g]	n.d.[g]	0.085	60.3	647	0.026	18.1	687

[a] uncertainties in the measurements are shown in Table S5.

[b] data for the WT complexes are taken from (E:FOL)[77], (E:FOL:NADP$^+$),[43] (E:THF:NADP$^+$),[45] and D.D. Boehr, unpublished, and (E:THF:NADPH).[45]

[c] the location of the residues showing conformational exchange in the `active-site' (including active-site loops, cofactor-binding cleft and/or substrate/product binding pocket) depends heavily on the specific complex (see[45] and Figure 7)

[c] not determined. Conformational exchange is apparent but could not be satisfactorily fit to k_{ex} and/or p_{APB}

[d] residues in the cofactor binding site were excluded from the cluster 1 fit (see text)

[e] not determined. Conformational exchange is apparent but could not be appropriately fit to k_{ex} and/or p_{APB}

[f] there are three regions of protein dynamics in the WT E:THF:$NADP^+$ complex that have different k_{ex} and p_{APB}: the active-site loops, the cofactor-binding cleft and the C-terminal associated region. The k_{ex} and p_{APB} values for the cofactor-binding cleft are in brackets.

[g] not determined. Data for WT or G121V complex were not collected at this temperature.

Table 2

Comparison of thermodynamics parameters for WT and Gly121Val DHFR μs-ms timescale dynamics at 300 K

Thermodynamic Parameter (kcal/mol)	[a] WT E:FOL:NADP$^+$ Closed → Occluded	[a] WT E:THF:NADP$^+$ Occluded → Closed	G121V E:FOL:NADP$^+$ Occluded → ?
Energetic differences between higher energy and ground-state conformations			
ΔG	2.1 ± 0.3	2.7 ± 0.5	1.7 ± 0.0
ΔH	15.6 ± 2.1	13.9 ± 0.5	4.7 ± 0.4
TΔS	13.5 ± 2.1	11.2 ± 0.5	3.0 ± 0.4
Activation energy barrier parameters			
$\Delta G^{\ddagger}$	16.0	15.9 ± 0.5	15.8 ± 0.1
$\Delta H^{\ddagger}$	21.2	20.3 ± 0.5	17.3 ± 1.9
$T\Delta S^{\ddagger}$	5.1	4.4 ± 0.5	1.5 ± 1.8

[a] data for the WT complexes are taken from (E:FOL:NADP$^+$)[43] and E:THF:NADP$^+$ (D.D. Boehr, unpublished)